

Correlation enhancement of high-order harmonics generation in Xe

Alexander W. Bray,¹ David Freeman,¹ Sebastian Eckart,² and Anatoli S. Kheifets¹

¹*Research School of Physics and Engineering, The Australian National University, Canberra ACT 0200, Australia*

²*Institut für Kernphysik, Goethe-Universität, Max-von-Laue-Str. 1, 60438 Frankfurt, Germany*

(Dated: March 18, 2022)

We consider the process of high-order harmonics generation (HHG) in the xenon atom enhanced by the inter-shell correlation between the valence $5p$ and inner $4d$ shells. We derive the HHG spectrum from a numerical solution of the one-electron time-dependent Schrödinger equation multiplied by the enhancement factor taken as the photoionization cross-sections ratio calculated with and without the inter-shell correlation. Such a simplified approach is adequate to describe the experimental HHG spectrum reported by Shiner *et al.* [Nat. Phys. **7**, 464 (2011)] generated by a single color IR laser. Similarly, we find good agreement when applied to the two-color driven HHG spectra reported by Faccialá *et al.* [Phys. Rev. Lett. **117**, 093902 (2016)].

PACS numbers: 32.80.Rm, 32.80.Fb, 42.50.Hz

I. INTRODUCTION

The inter-shell correlation in atomic photoionization is a well documented phenomenon [1]. Instead of directly removing an electron from a designated atomic shell, the photon can be absorbed by an adjacent, inner or outer, shell. The photoelectron then either scatters inelastically on the ionized core, or recombines with its parent ion. In the latter, the released energy is transferred to remove an electron from said atomic shell. Such an inter-shell correlation can modify very considerably the photoionization cross-section (PICS) in a given atomic shell. In the Xe atom, the outer $5p$ PICS is significantly enhanced by the correlation with the inner $4d$ shell near the so-called giant resonance [2]. This resonance is formed when the outgoing photoelectron is trapped in a combined field of the Coulomb potential of the residual ion and the centrifugal potential. This process leads to enhancement of the $5p$ PICS which can exceed an order of magnitude. Not surprisingly, a similar correlation enhances the HHG spectrum of Xe in the same photon energy range [3–5]. Indeed, the photorecombination, the last stage of the three-step picture of the HHG process [6], is the inverse to photoionization and their respective cross-sections are related through the principle of detailed balance. This principle was first applied in the modelling of HHG by Morishita *et al.* [7] and forms the basis of the Quantitative Rescattering (QRS) [8] approach. In which, the spectra is determined by the returning electron wavepacket multiplied by the corresponding dipole transition amplitude. For a comprehensive application of the QRS method to single-color HHG from Xe accounting for propagation effects and further experimental parameters the readers are referred to [9, 10]. Under this same factorization, analytic expressions for the high-energy end of the HHG plateau were derived by Frolov *et al.* [11, 12, 13].

Our theoretical treatment of the correlation enhanced HHG spectrum of Xe is similarly based on this principle. First, the HHG spectrum of Kr was recorded in the

spectral range free from resonant enhancement [3, 14]. Then this spectrum was normalized to the experimental PICS of the $4p$ shell in the polarization direction $\sigma_z(4p) = \sigma_{4p}(1 + \beta_{4p})$, σ being the total PICS and β the angular anisotropy parameter. The proportionality factor was found to be virtually flat as a function of the photon energy. Then this factor was multiplied by the experimental PICS $\sigma_z(5p)$ and compared with the recorded HHG spectrum of Xe. The comparison proved very convincing. Subsequent, more refined, theoretical treatment within the strong-field approximation [15] and the time-dependent R -matrix theory [16, 17] confirmed this analysis.

In the more recent measurements [4, 5], the correlation enhanced HHG spectrum of Xe was recorded using the two-color $\omega/2\omega$ IR laser field. This spectrum was systematically studied as a function of the relative $\omega/2\omega$ phase which allowed for a tunable enhancement of a narrow spectral range to be overlapped with the giant resonance of Xe. Comparison was made with the solution of the time-dependent Schrödinger equation (TDSE) expanded on the specially designed configuration-interaction basis (the so-called time-dependent configuration-interaction singles - TDCIS) [18]. As expected, the HHG spectral range of the giant resonance was greatly amplified, both by the phase tuning and the inter-shell correlation. Agreement with the TDCIS calculation was achieved only when the intershell correlation between the $5p$, $5s$ and $4d$ shells was taken into account. However, there was a noticeable disagreement around 63 eV photon energy discussed both in [4] and [5] and attributed to interference between the various photoelectron trajectories recombining with the parent ion from the opposite sides. It was concluded that this interference was blurred in the experiment due to a likely spatial and temporal averaging effects.

In the present work, we consider both the single-color and two-color driven HHG spectra of Xe within the same theoretical model. We derive the HHG spectrum from a numerical solution of the one-electron TDSE multiplied by the enhancement factor. This factor is taken

as the PICS ratio calculated with and without the $5p/4d$ inter-shell correlation. We find this approach to work for both the single-color driven HHG as was previously documented [3], and the two-color field with the additional phase dependency introduced.

II. METHODS

A. One-electron TDSE and HHG spectrum

As previously [19, 20], we solve the one-electron TDSE for a target atom

$$i\partial\Psi(\mathbf{r},t)/\partial t = [\hat{H}_{\text{atom}} + \hat{H}_{\text{int}}(t)]\Psi(\mathbf{r},t), \quad (1)$$

where the radial part of the atomic Hamiltonian

$$\hat{H}_{\text{atom}}(r) = -\frac{1}{2}\frac{d^2}{dr^2} + \frac{l(l+1)}{2r^2} + V(r) \quad (2)$$

contains an effective one-electron potential $V(r)$ (Kr [21], Xe [20]).

The Hamiltonian $\hat{H}_{\text{int}}(t)$ describes interaction with the external field and is written in the velocity gauge

$$\hat{H}_{\text{int}}(t) = \mathbf{A}(t) \cdot \hat{\mathbf{p}}, \quad \mathbf{E}(t) = -\partial\mathbf{A}(t)/\partial t. \quad (3)$$

This external field is given by

$$A_z(t, \alpha, \phi) = -A_{z0}f(t)[\sin\omega t + \alpha\sin(2\omega t + \phi)]. \quad (4)$$

The $f(t)$ is a Gaussian envelope of the form given in [22]. In the one-color case ($\alpha = 0$) we set these parameters to correspond to a 1800 nm pulse of peak intensity 1.8×10^{14} W/cm² and FWHM approximately 8.8 fs with respect to this intensity. For the two-color case we take the ω (1550 nm) field to be of FWHM 25 fs with 7×10^{13} W/cm² peak intensity, and the electric field strength of the 2ω (775 nm) to be 0.4 of that of the primary.

Once the time-dependent wave function $\Psi(r, t)$ is obtained, the induced dipole moment in the length and acceleration forms can be calculated [23]:

$$d_L(t) = \langle \Psi(t) | z | \Psi(t) \rangle \quad (5)$$

$$d_A(t) = \langle \Psi(t) | -dV(r)/dz + E(t) | \Psi(t) \rangle \quad (6)$$

where z is the displacement along the laser polarisation axis. The HHG power spectra can be obtained by the Fourier transformation of time-dependent dipole moment, it is expressed as

$$P_L(\omega) \propto \omega^4 \left| \int_{-T/2}^{T/2} d_L(t) e^{-i\omega t} dt \right|^2 \quad (7)$$

$$P_A(\omega) \propto \left| \int_{-T/2}^{T/2} d_A(t) e^{-i\omega t} dt \right|^2 \quad (8)$$

for a pulse of length T . Typically the dipole acceleration form, when applicable, is preferred as it is not influenced by flux far from the origin, and hence is more rapidly convergent. This is the case for our calculations and accordingly, what we use.

It should also be noted that theoretical spectra as derived above exhibit sharp oscillations over several orders of magnitude at an energy resolution unattainable by experiment. Consequently, for comparison, filtering techniques are applied to the theoretical spectrum designed to mimic experimental detection. For this purpose we choose Gaussian convolution of the form

$$P^S(\omega) = \frac{\int_0^\infty P(\omega') e^{-\sigma(\omega-\omega')^2} d\omega'}{\int_0^\infty e^{-\sigma(\omega-\omega')^2} d\omega'}, \quad (9)$$

with $\sigma = 0.01$. In practice, the upper integration bound is the highest photon energy in the theoretical spectrum. The effect of such convolution is demonstrated for our single color Kr calculation in Fig. 1.

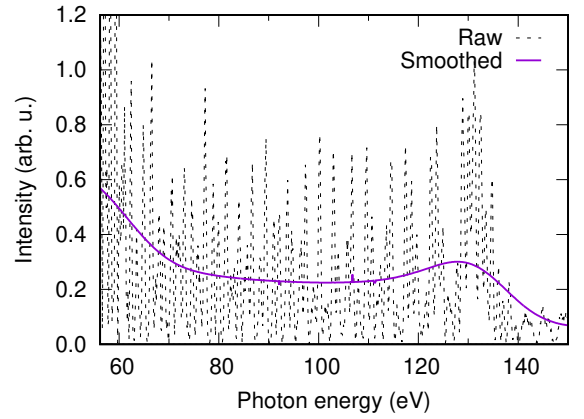


FIG. 1: (Color online) Comparison between the raw theoretical HHG spectrum (8) (dashed black line) and that smoothed via Gaussian convolution (9) (blue solid line). The spectra in particular are for the single color case on Kr.

It should also be noted that comparison with experiment is further complicated by macroscopic propagation effects through the medium whereas theory typically provides only the single atom response. Accordingly however, experiments are conducted with thin targets to minimize such macroscopic effects [3].

B. Inter-shell correlation

Random phase approximation with exchange (RPAE) has long been used to treat inter-shell correlations in noble gas atoms [1]. In this approximation, the two inter-shell correlation processes are considered: recombination and inelastic electron scattering. These processes contain the direct and exchange matrix elements of the Coulomb interaction which is highlighted in the acronym RPAE. The photoionization amplitude calculated in the RPAE contains the three terms shown graphically in Fig. 2.

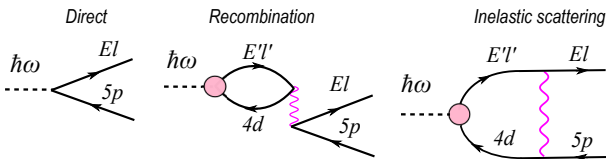


FIG. 2: (Color online) Graphical representation of the direct (left) and correlation (center and right) photoionization processes included in the RPAE. Straight lines with arrows to the right/left represent a photoelectron/hole. The dashed line exhibits a photon and the wavy line displays the Coulomb interaction. The dashed circle indicates summation of direct and exchange correlation processes to infinite order. The arrow direction corresponds to photoionization and is the reverse in the case of HHG.

In the $5p/4d$ intershell correlation of Xe considered here, the direct term corresponds to the removal of the electron from the valence shell and creation of the $5p$ hole. In the recombination process, the photon is absorbed by the inner shell and the $4d$ hole is created initially. Then this hole recombines with the photoelectron and the Coulomb interaction ejects an electron from the outer $5p$ shell. In the inelastic scattering process, the photoelectron scatters on the $4d$ hole and promotes it to the $5p$ state. Thus the final state in all three processes is identical and the corresponding photoionization amplitudes should be added coherently. The direct photoionization amplitude in Fig. 2 contains the matrix element of the dipole electromagnetic operator acting on the Hartree-Fock bound and continuous states. The correlation amplitudes contain an infinite sum of the matrix elements driven by the dipole electromagnetic operator and containing the Coulomb interaction to infinite order.

Relativistic extension of random phase approximation (RRPA) [24] has been developed to treat heavier atoms. It accounts for the same direct and exchange correlation processes exhibited in Fig. 2 but the acronym RRPA does not highlight the exchange for brevity. The relativistic basis of the one-electron states contains the Dirac-Fock orbitals, bound and continuous.

We define the $5p/4d$ correlation enhancement factor as the ratio of the polarization direction PICS calculated with and without inter-shell correlation. Both the PICS and β parameters are calculated in the RPAE and RRPA by summation of all the three amplitudes shown in Fig. 2. While the correlation-free PICS and β are obtained from the direct amplitude only.

For completeness, we also consider the correlation enhanced photoionization of Xe calculated within the relativistic time-dependent density functional theory (RTDDFT) [25]. The correlation free calculation in this work is performed using the relativistic Kohn-Sham (RKS) orbitals. Both the PICS and the β parameters are presented in the RTDDFT and RKS and hence the polarization direction PICS can be evaluated both with and without inter-shell correlation.

III. RESULTS AND DISCUSSION

A. Enhancement factor

The correlation enhancement factor is calculated as the PICS ratio

$$\rho(\omega) = \sigma_z^{5p/4d}(\omega) / \sigma_z^{5p}(\omega), \quad (10)$$

where $\sigma_z^{5p/4d}$ refers to the polarization direction PICS calculated with the account for the $5p/4d$ inter-shell correlation whereas $\sigma_z^{5p}(\omega)$ is calculated without such a correlation. The non-correlated RRPA, RPAE and RTDDFT calculations employ different one-electron basis sets. These bases are not necessarily commensurate with the one-electron TDSE. Even though we selected the one-electron potential in Eq. (1) carefully, an additional test is needed to make sure we can apply various correlation enhancement factors to the TDSE generated HHG spectrum. In this test, we compare the angular anisotropy β parameters derived from non-correlated RRPA and RKS calculations. We further compare with the parameters resulting from our choice of Xe pseudopotential (labelled TDSE) obtained from the angular dependence of the photoelectron spectrum as described in [19]. Results of all these calculations are shown in Fig. 3. Even though numerically the β parameters differ, the general trend of their energy dependence is very similar in all the calculations.

In Fig. 4 we present the polarization direction PICS enhanced by the correlation $\sigma_z^{5p/4d}$ returned by different calculations, RRPA, RPAE and RTDDFT, and compare them with the experimental values collated in [3]. It appears that the RRPA calculation is closest to the experiment.

Finally, we proceed with the correlation enhancement factor calculation. This factor is displayed in Fig. 5.

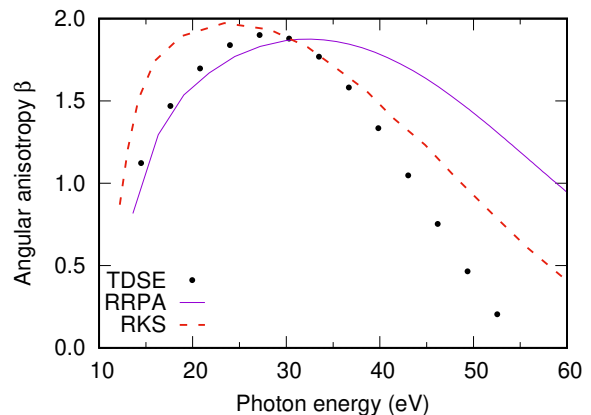


FIG. 3: (Color online) The angular anisotropy parameters (β) resulting from the harmonic peaks of our TDSE (black points), and RRPA calculations (blue solid line), and from RKS [25] (red dashed line).

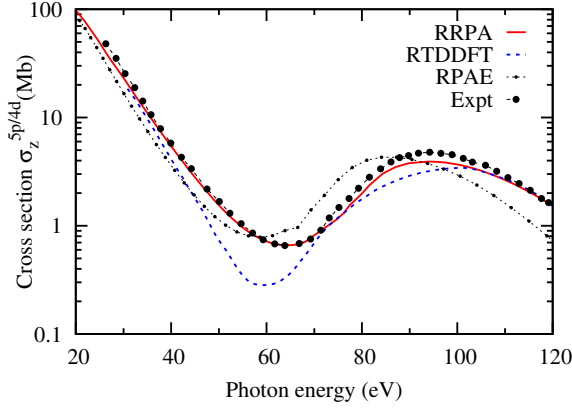


FIG. 4: (Color online) The polarization direction photoionization cross-section (PICS) $\sigma_z(5p) = \sigma_{5p}(1 + \beta_{5p})$. The (red) solid line - our RRPA calculation, the (blue) dashed line - RTDDFT [25], the dot-dashed line - our RPAE calculation, the filled circles - experimental data compiled in [3] and renormalized to RRPA.

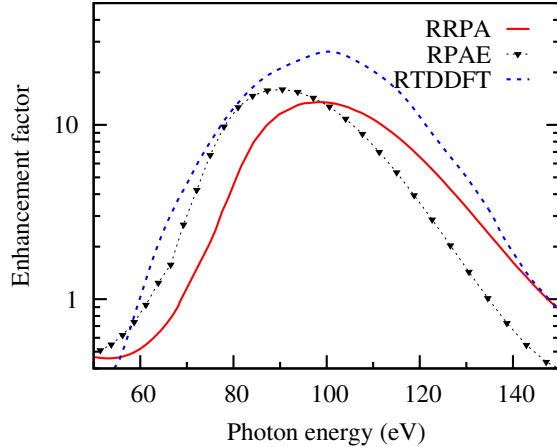


FIG. 5: (Color online) The correlation enhancement factor Eq. (10) from our RRPA calculation (red solid line), our RPAE calculation (black dotted line with triangles), and the RTDDFT (blue dashed line) [25].

B. Single color

As the first test of our computational procedure we calculate the HHG spectrum of Kr, as is unaffected by the correlation enhancement. We make a comparison with the experiment [3, 14] and the *R*-matrix calculation [16]. The calculated spectrum derived from Eqs. (1), (6) and (8) and smoothed by a Gaussian convolution (9) is shown by the green dashed line in the top frame of Fig. 6. This compares favourably both with the experiment [3] (green line) and against an analogous *R*-matrix calculation [16] (blue dashed line). This is in particularly true for the location of the spectral cut-off albeit the relative magnitude of the experiment is marginally higher. All

three datasets have approximately equal predictions for the Cooper minimum.

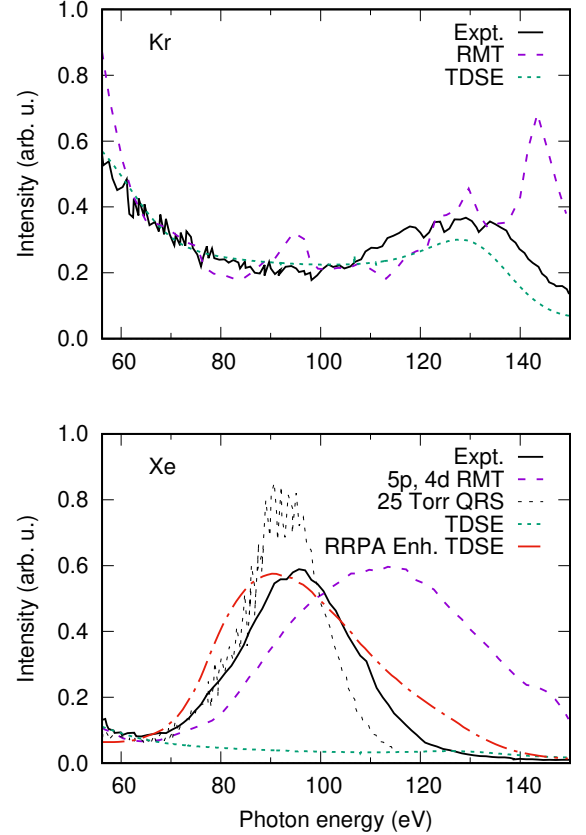


FIG. 6: (Color online) Top: The HHG spectrum of Kr from experiment [3] (black solid line), *R*-matrix calculation [16] (blue sparse dashed line), and our present TDSE theory (green dense dashed line). Bottom: As above for Xe with the addition of our RRPA enhanced TDSE theory (red dash-dotted line) and QRS calculation [10] (black thin dashed line).

To test our enhancement procedure, we calculate single color HHG spectrum from Xe. Our results are given in the bottom frame of Fig. 6 as enhanced (red dot-dashed line) and otherwise (green dashed line) and compared again with experiment [3] (black solid line) and *R*-matrix calculation [16] (blue dashed line). Additionally we include the QRS 25 Torr dataset from Fig. 3c of [10] given for peak intensity 2×10^{14} W/cm². This latter approach includes macroscopic effects introducing dependencies on the focusing position and gas pressure. Of the QRS calculations presented [9, 10] it is this which appears to have best agreement with the Shiner experiment. Our reproduction of the giant resonance is an improvement over the RMT method. However, both of these approaches exhibit a broader tail at high energies than that seen in the experiment. Conversely, the QRS method places the resonance well in-line with the experiment but with an altogether sharper dependency.

C. Two color

We now look to calculate the two-color HHG spectra of Xe presented in [4]. The present TDSE calculated HHG spectra, both raw and enhanced by the RRPA $5p/4d$ intershell correlation, are displayed in the middle and bottom frames of Fig. 7 respectively. They are drawn as 2D false color plots in the energy and relative phase ϕ coordinates. The top frame of Fig. 7 exhibits the experiment from [5]. We find solid qualitative agreement between our results and that of the experiment, and as desired, applying the enhancement ratio appropriately magnifies the caustic in the cut-off region. The most notable difference is the differing phase at which the low energy maxima occurs, being approximately $\phi = 0.75\pi$ in the experiment and our theory predicting closer to 0.10π below this. Additionally the experiment exhibits a much stronger relative background across phases than what we see in our calculation. This being a feature similarly found in their comparison with TDCIS theory [4].

A more detailed comparison is made in Fig. 8 where the phase maximum of the spectra shown in Fig. 7 is traced ($\max_{\phi} P_A$). On the top panel we display the TDSE calculation compared with the uncorrelated ($5p$ only) TDCIS theory. Here we find the observed trend to be essentially equivalent bar minor features. On the bottom panel comparison is made of between our RRPA enhanced spectra and the correlated TDCIS ($5p$, $4d$, $5s$) as well as the experiment. Again we find very solid agreement between all three datasets. Most notably, we did not find a noticeable disagreement between our calculation and the experiment around 63 eV photon energy which is visible in the TDCIS calculation.

IV. CONCLUSIONS

We performed simulations of HHG spectra from Xe in both one- and two-color fields from the numerical solution of the one-electron TDSE and account for the effects of intershell correlation as a ratio of photoionization cross-sections. In both cases we find strong agreement between our results and those of experiment and to either be an improvement, or equivalently accurate, to those of more advanced theories. This is attributed to the equivalence of the recombination process in the production of HHG to the time reversal of photoionization and accordingly find the correlation effects to behave similarly, even when the dynamics is complicated significantly by the introduction of the secondary field. Such an observation suggests further aspects of two-color HHG production can be efficiently and effectively studied through the lens of correlated photoionization.

To this end, we will next apply our techniques to other atomic systems where the HHG process is enhanced by inter-shell correlation and giant resonances. One such system is atomic manganese where a giant autoionization resonance due to transition from the $3p$ to a partially

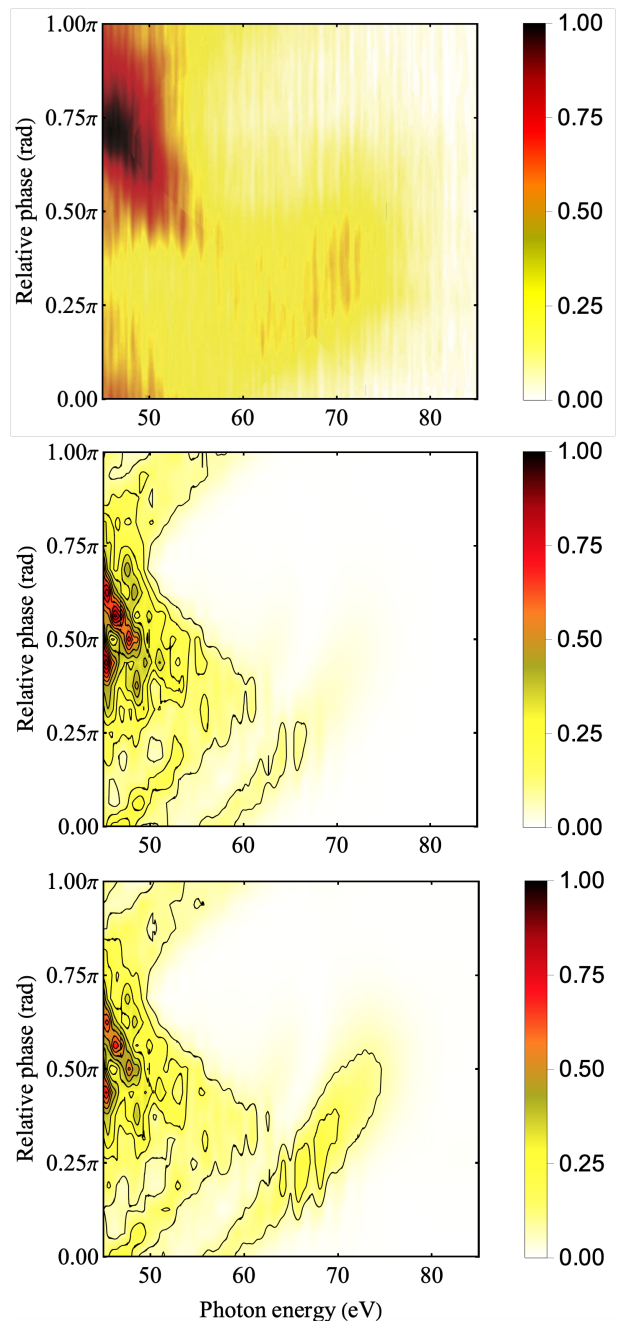


FIG. 7: (Color online) The HHG spectrum of Xe recorded as a function of the photon energy and the relative phase ϕ in Eq. (4). Top: Experimental spectra from [5]. Middle: Present TDSE calculation. Bottom: TDSE spectra enhanced by RRPA. Contours connect regions of equal intensity in intervals of approximately 7%.

filled $3d$ shell enhances strongly photoionization and photorecombination from the outer valence shell. This enhancement is recorded in the HHG spectrum accordingly [26].

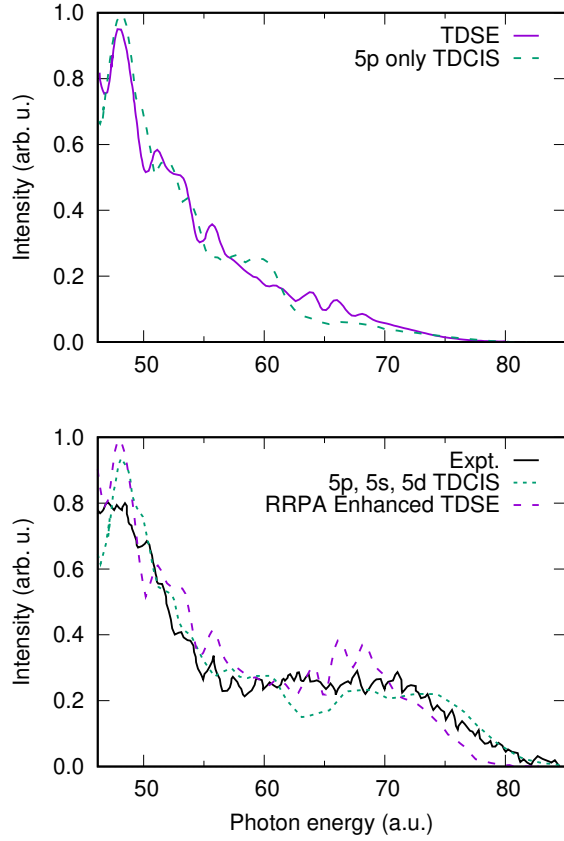


FIG. 8: (Color online) The maximum HHG yield of Xe with phase for a given photon energy ($\max_{\phi} P_A$). Top: Our raw TDSE compared with the 5p only TDCIS theory [4]. Bottom: Enhanced TDSE result compared with the correlated TDCIS theory and experimental measurements [4].

Acknowledgements

The authors are greatly indebted to Serguei Patchkovskii who placed his iSURF TDSE code at their disposal. They are also thankful to Soumyajit Saha for his help with the RRPA calculations and to XuanYang Lai for many stimulating discussions. Resources of the National Computational Infrastructure (NCI Australia) were employed.

-
- [1] M. Y. Amusia, *Atomic photoeffect* (Plenum Press, New York, 1990).
- [2] J. P. Connerade, J. E. Esteve, and R. Karnatak, eds., *Giant Resonance in Atoms, Molecules and Solids* (Plenum, New York, 1986), no. 151 in Nato Science Series B.
- [3] A. D. Shiner, B. E. Schmidt, C. Trallero-Herrero, H. J. Worner, S. Patchkovskii, P. B. Corkum, J. C. Kieffer, F. Legare, and D. M. Villeneuve, *Probing collective multi-electron dynamics in xenon with high-harmonic spectroscopy*, Nat Phys **7**, 464 (2011), 10.1038/nphys1940.
- [4] D. Faccialà, S. Pabst, B. D. Bruner, A. G. Ciriolo, S. De Silvestri, M. Devetta, M. Negro, H. Soifer, S. Stagira, N. Dudovich, et al., *Probe of multielectron dynamics in xenon by caustics in high-order harmonic generation*, Phys. Rev. Lett. **117**, 093902 (2016).
- [5] D. Faccialà, S. Pabst, B. D. Bruner, A. G. Ciriolo, M. Devetta, M. Negro, P. P. Geetha, A. Pusala, H. Soifer, N. Dudovich, et al., *High-order harmonic generation spectroscopy by recolliding electron caustics*, J. Phys. B **51**(13), 134002 (2018).
- [6] P. B. Corkum, *Plasma perspective on strong field multi-photon ionization*, Phys. Rev. Lett. **71**, 1994 (1993).
- [7] T. Morishita, A.-T. Le, Z. Chen, and C. D. Lin, *Accurate retrieval of structural information from laser-induced photoelectron and high-order harmonic spectra by few-cycle laser pulses*, Phys. Rev. Lett. **100**, 013903 (2008).
- [8] C. Lin, A.-T. Le, C. Jin, and H. Wei, *Elements of the quantitative rescattering theory*, Journal of Physics B: Atomic, Molecular and Optical Physics **51**(10), 104001 (2018).
- [9] C. Jin, A.-T. Le, C. A. Trallero-Herrero, and C. D. Lin, *Generation of isolated attosecond pulses in the far field by spatial filtering with an intense few-cycle mid-infrared laser*, Phys. Rev. A **84**, 043411 (2011).
- [10] C. Trallero-Herrero, C. Jin, B. Schmidt, A. Shiner, J. Kieffer, P. Corkum, D. Villeneuve, C. Lin, F. Légaré, and A.-T. Le, *Generation of broad xuv continuous high harmonic spectra and isolated attosecond pulses with intense mid-infrared lasers*, Journal of Physics B: Atomic, Molecular and Optical Physics **45**(1), 011001 (2011).
- [11] M. V. Frolov, N. L. Manakov, T. S. Sarantseva, M. Y. Emelin, M. Y. Ryabikin, and A. F. Starace, *Analytic description of the high-energy plateau in harmonic generation by atoms: Can the harmonic power increase with increasing laser wavelengths?*, Phys. Rev. Lett. **102**, 243901 (2009).
- [12] M. V. Frolov, N. L. Manakov, A. A. Silaev, N. V. Vvedenskii, and A. F. Starace, *High-order harmonic generation by atoms in a few-cycle laser pulse: Carrier-envelope phase and many-electron effects*, Phys. Rev. A **83**, 021405 (2011).
- [13] M. V. Frolov, N. L. Manakov, T. S. Sarantseva, and A. F. Starace, *High-order-harmonic-generation spectroscopy with an elliptically polarized laser field*, Phys. Rev. A **86**, 063406 (2012).
- [14] A. D. Shiner, B. E. Schmidt, C. Trallero-Herrero, P. B. Corkum, J.-C. Kieffer, F. Legar., and D. M. Villeneuve, *Observation of Cooper minimum in krypton using high harmonic spectroscopy*, J. Phys. B **45**(7), 074010 (2012).
- [15] S. Patchkovskii, O. Smirnova, and M. Spanner, *Attosecond control of electron correlations in one-photon ionization and recombination*, J. Phys. B **45**(13), 131002 (2012).
- [16] O. Hassouneh, A. C. Brown, and H. W. van der Hart, *Harmonic generation by noble-gas atoms in the near-IR regime using ab initio time-dependent R-matrix theory*, Phys. Rev. A **90**, 043418 (2014).
- [17] L. Moore, M. Lysaght, L. Nikolopoulos, J. Parker, H. van der Hart, and K. Taylor, *The RMT method for many-electron atomic systems in intense short-pulse laser light*, Journal of Modern Optics **58**(13), 1132 (2011).
- [18] S. Pabst and R. Santra, *Strong-field many-body physics and the giant enhancement in the high-harmonic spectrum of xenon*, Phys. Rev. Lett. **111**, 233005 (2013).
- [19] A. W. Bray, F. Naseem, and A. S. Kheifets, *Simulation of angular-resolved RABBITT measurements in noble-gas atoms*, Phys. Rev. A **97**, 063404 (2018).
- [20] A. W. Bray, F. Naseem, and A. S. Kheifets, *Photoionization of Xe and Xe@C₆₀ from the 4d shell in RABBITT fields*, Phys. Rev. A **98**, 043427 (2018).
- [21] F. Cloux, B. Fabre, and B. Pons, *Semiclassical description of high-order-harmonic spectroscopy of the Cooper minimum in krypton*, Phys. Rev. A **91**, 023415 (2015).
- [22] S. Patchkovskii and H. Muller, *Simple, accurate, and efficient implementation of 1-electron atomic time-dependent schrödinger equation in spherical coordinates*, Computer Physics Communications **199**, 153 (2016).
- [23] K. Burnett, V. Reed, J. Cooper, and P. Knight, *Calculation of the background emitted during high-harmonic generation*, Physical Review A **45**(5), 3347 (1992).
- [24] W. R. Johnson and C. D. Lin, *Multichannel relativistic random-phase approximation for the photoionization of atoms*, Phys. Rev. A **20**, 964 (1979).
- [25] D. Toffoli, M. Stener, and P. Decleva, *Application of the relativistic time-dependent density functional theory to the photoionization of xenon*, J. Phys. B **35**(5), 1275 (2002).
- [26] M. A. Fareed, V. V. Strelkov, M. Singh, N. Thiré, S. Mondal, B. E. Schmidt, F. Légaré, and T. Ozaki, *Harmonic generation from neutral manganese atoms in the vicinity of the giant autoionization resonance*, Phys. Rev. Lett. **121**, 023201 (2018).